

# Why and How: Knowledge-Guided Learning for Cross-Spectral Image Patch Matching

Chuang Yu<sup>1,2,3</sup>, Yunpeng Liu<sup>2,\*</sup>, Jinmiao Zhao<sup>1,2,3</sup>, Xiangyu Yue<sup>4,\*</sup>

<sup>1</sup>Key Laboratory of Opto-Electronic Information Processing, Chinese Academy of Sciences

<sup>2</sup>Shenyang Institute of Automation, Chinese Academy of Sciences

<sup>3</sup>University of Chinese Academy of Sciences

<sup>4</sup>MMLab, The Chinese University of Hong Kong

## Abstract

Recently, cross-spectral image patch matching based on feature relation learning has attracted extensive attention. However, performance bottleneck problems have gradually emerged in existing methods. To address this challenge, we make the first attempt to explore a stable and efficient bridge between descriptor learning and metric learning, and construct a knowledge-guided learning network (KGL-Net), which achieves amazing performance improvements while abandoning complex network structures. Specifically, we find that there is feature extraction consistency between metric learning based on feature difference learning and descriptor learning based on Euclidean distance. This provides the foundation for bridge building. To ensure the stability and efficiency of the constructed bridge, on the one hand, we conduct an in-depth exploration of 20 combined network architectures. On the other hand, a feature-guided loss is constructed to achieve mutual guidance of features. In addition, unlike existing methods, we consider that the feature mapping ability of the metric branch should receive more attention. Therefore, a hard negative sample mining for metric learning (HNSM-M) strategy is constructed. To the best of our knowledge, this is the first time that hard negative sample mining for metric networks has been implemented and brings significant performance gains. Extensive experimental results show that our KGL-Net achieves SOTA performance in three different cross-spectral image patch matching scenarios. Our code are available at <https://github.com/YuChuang1205/KGL-Net>.

## 1. Introduction

Image patch matching aims to measure the similarity between image patches and is widely used in image registration [1-3], image retrieval [4-6], and re-identification [7-9]. Considering that a single-spectral image source often has limitations, cross-spectral image matching can establish the correspondence between different spectral images, laying the foundation for fully utilizing the complementary information [10, 11]. Compared with single-spectral image patch matching, cross-spectral image patch matching not only needs to faces illumination changes and geometric changes, but also has to

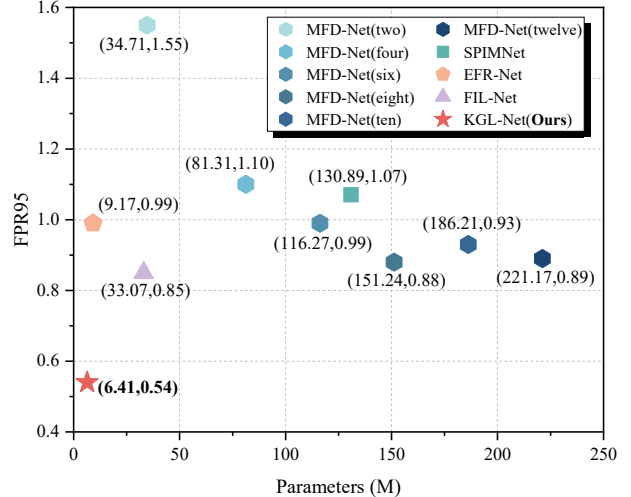


Figure 1. Comparison of different cross-spectral image patch matching methods on the VIS-NIR patch dataset. Our KGL-Net achieves an amazing performance improvements. Compared with the latest FIL-Net [1], KGL-Net reduces the FPR95 by **36.5%** (from 0.85 to 0.54). Compared with the lightweight EFR-Net [15], KGL-Net reduces the parameters by **30.1%** (from 9.17 to 6.41).

overcome the pixel-level nonlinear differences between cross-spectral image patches [1, 12-15]. Therefore, it is challenging to construct a high-performance cross-spectral image patch matching method.

Early image patch matching methods are based on non-deep learning methods, which mainly study grayscale information [16-19] or hand-crafted descriptors [20-29]. However, this type of method is seriously affected by hyperparameters and lacks robustness for complex scenarios. Compared with non-deep learning-based methods, deep learning-based methods can automatically learn the nonlinear mapping between input images and true labels [30], which has greater adaptability. Deep learning-based image patch matching methods include descriptor learning methods [31-43] and metric learning methods [1, 10, 12-15, 44-49]. Owing to the structural characteristics of these two methods, research on descriptor learning methods focuses on optimizing loss function [31-36, 40-43] and difficult sample mining [37-39, 41], whereas research on metric learning methods focuses on the design of network structures to mine more sufficient and

comprehensive feature relations between image patches [1]. The former has the characteristics of lightweight network but low accuracy. The latter has the characteristics of high accuracy but bloated network. Considering that matching accuracy is taken as the priority metric, existing cross-spectral image patch matching methods focus on metric learning [1, 12-15, 47, 49]. However, as shown in Fig. 1, although researchers have made great efforts in recent years, performance bottleneck problems have emerged.

To address this problem, we consider that we should break away from the inertial thinking of building more complex feature relation extraction network structures. Combining the advantages of descriptor learning [43], we make the first attempt to build a stable and efficient bridge between descriptor learning and metric learning. Unlike existing methods that focus on the design of feature extraction networks, we consider that the feature mapping ability of the metric branch should receive more attention. Considering that the metric branch is essentially a learnable discriminator, its ability is directly related to the input training data. Therefore, we make the first attempt to implement hard negative sample mining for metric learning. However, this seems impossible because of the input form and structural characteristics of the metric network. But nothing is impossible, just do it. On the one hand, we break the existing metric learning methods that directly use uniform and fixed positive and negative sample pairs, and use only positive sample pairs as inputs. This provides the basic conditions for hard negative sample mining. On the other hand, considering that the metric network uses the metric branch to combine the two-branch features [44, 45], it is unrealistic to directly perform hard negative sample mining. Through continuous exploration, we find that there is feature extraction consistency between metric learning based on feature difference learning and descriptor learning based on Euclidean distance. They all focus on extracting the differential features of the image patch itself relative to other image patches. Based on this, a hard negative sample mining for metric learning (HNSM-M) strategy is constructed, which cleverly uses the feature distance matrix generated by descriptor learning to guide metric learning to achieve effective hard negative sample mining. In addition, to ensure the stability and efficiency of the bridge, on the one hand, we fully explore 20 combined network architectures of descriptor learning and metric learning. On the other hand, we construct a feature-guided loss to achieve effective mutual guidance of features. The contributions of this study are summarized as follows:

(1) To solve the performance bottleneck in the current research, we make the first attempt to explore a stable and efficient bridge between descriptor learning and metric learning and construct a KGL-Net, which achieves amazing performance improvements while abandoning complex network structures.

(2) We find that there is feature extraction consistency between metric learning based on feature difference learning and descriptor learning based on Euclidean distance. To ensure the stability and efficiency of the constructed bridge, we not only conduct an in-depth exploration of 20 combined network architectures, but also a feature-guided loss is constructed to achieve mutual guidance of features.

(3) We focus on improving the feature mapping capability of the metric branch and construct a HNSM-M strategy. To the best of our knowledge, this is the first time that hard negative sample mining for metric networks is implemented and brings significant performance gains.

## 2. Related Work

**Descriptor Learning Methods** [31-43] use neural networks to extract high-level image patch features and measure their similarity by feature distance. Existing research focuses on optimizing loss functions [31-36, 40-43] and sampling strategies [37-39, 41]. In terms of the loss functions, hinge embedding loss [31] and triplet loss [32, 33] are commonly used. Unlike hinge embedding loss, which uses absolute distance, triplet loss is optimized based on relative distance, which is more stable. Therefore, subsequent research focuses on triplet loss and its variants [32-36, 40-43]. In terms of the sampling strategy, the early L2-Net [41] proposes a progressive sampling method that can generate many negative samples. However, these negative samples are mostly simple samples, which are difficult to provide effective feedback for network training. Therefore, subsequent research gradually turned to the design of effective hard negative sample mining strategies [37-39]. However, owing to the structural limitations of descriptor learning, it cannot effectively model the relations between image patches [1, 12-15]. This method has the advantages of being fast and lightweight, but the matching results are poor.

**Metric learning methods** [1, 10, 12-15, 44-49] extract and measure image patch features in sequence by using neural networks, which have flexible feature relation modelling capabilities. It focuses on the design of the network structure. MatchNet [44] is one of the earliest metric learning methods. Subsequently, Zagoruyko et al. [45] show that a 2-channel network that directly calculates feature similarity based on a fused feature space has better matching performance than the Siamese network and Pseudo-Siamese network. The above metric learning methods are designed for single-spectral image patch matching. Cross-spectral image patch matching is more complex and its research is relatively late. Its early research is deeply inspired by single-spectral image matching methods. Inspired by [45], Aguilera et al. [10] propose the Siamese network, the Pseudo-Siamese network and the 2-channel network for cross-spectral image patch matching.

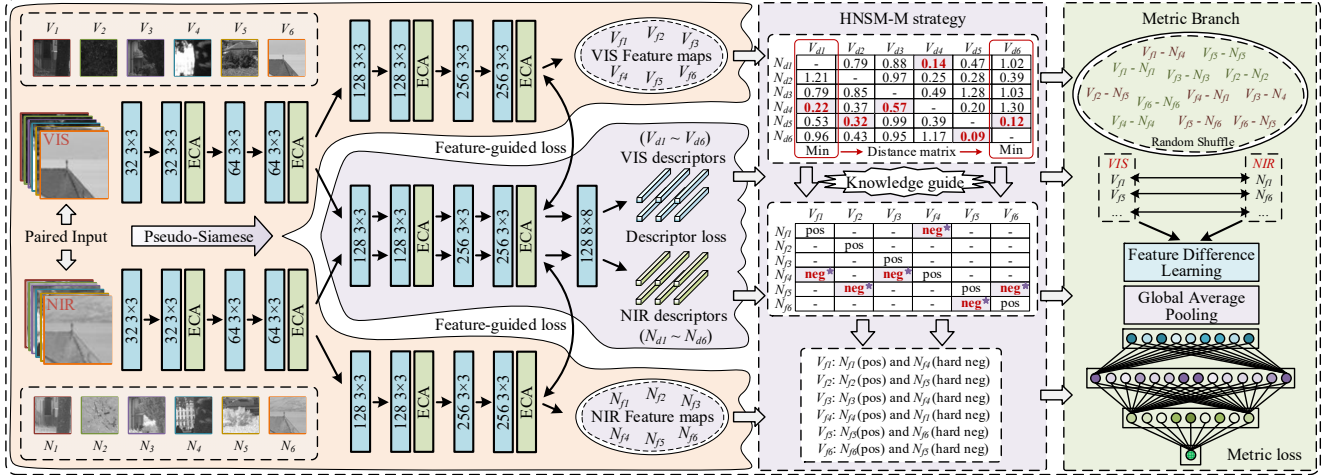


Figure 2. The overall structure of KGL-Net. Each blue block denotes a convolution operation, a Filter Response Normalization (FRN) [53], and a Thresholded Linear Unit (TLU) [53], where “ $n \ b \times b$ ” means that the number of channels of the output feature map is  $n$  and the convolution kernel size is  $b \times b$ . “ECA” denotes the efficient channel attention module [54].

Subsequently, SCFDM [47] extracts semantically invariant features of cross-spectral image patches in a shared semantic feature space and achieves significant performance improvement, which further reveals that the relation learning between image patch features is better than the learning of individual image patch features. Therefore, recent deep learning-based cross-spectral image patch matching methods [1, 12-15, 48, 49] all emphasize the extraction of diverse relations. However, existing research has gradually shown performance bottlenecks.

### 3. Methods

In this section, we will first elaborate our motivations to explain the “Why”. Then, we will elaborate on our proposed KGL-Net to explain “How”. The overall structure of KGL-Net is shown in Fig. 2.

#### 3.1. Motivation

**1) Performance bottleneck.** For the cross-spectral image patch matching task, existing methods focus on improving the feature extraction network part to mine more sufficient and comprehensive feature relations between image patches [1, 12-15, 47-49]. However, as the network becomes more complex, the improvement in matching results gradually levels off. From Fig. 1, compared with MFD-Net, FIL-Net only decreases the FPR95 by 3.4% (from 0.88 to 0.85). It is undeniable that once a certain level of performance is reached, further performance improvements become increasingly challenging. However, the performance bottleneck of existing methods is a real problem. Therefore, we make the first attempt to build a stable and efficient bridge between descriptor learning and metric learning to overcome this bottleneck without increasing resource consumption.

**2) Feature extraction consistency.** Through continuous research, we find that there is feature extraction consistency between metric learning based on feature difference learning [12] and descriptor learning based on Euclidean distance [13]. They all focus on extracting the differential features of the image patch itself relative to other image patches. Therefore, the features extracted by the feature extraction network parts of the two are similar. Taking a visible spectrum (VIS) image patch  $V_p$  and a near infrared (NIR) image patch  $N_p$  as examples, they are both passed through the feature extraction part of the metric network and the descriptor network, respectively:

$$(V_f, N_f) = \varphi_m(V_p, N_p) \quad (1)$$

$$(V'_f, N'_f) = \varphi_d(V_p, N_p) \quad (2)$$

Then, the extracted features are operated via the metric branch based on feature difference learning and the descriptor processing based on Euclidean distance:

$$S_{out} = \varphi'_m |V_f - N_f| \quad (3)$$

$$dist_{out} = \|V_d - N_d\|_2 = \|\varphi'_d \cdot V'_f - \varphi'_d \cdot N'_f\|_2 \quad (4)$$

where  $S_{out}$  is the similarity output by the metric network.  $dist_{out}$  is the distance output by the descriptor network.  $\varphi'_m$  denotes the metric branch network part.  $\varphi'_d$  denotes the network part in the descriptor network that converts high-level features into descriptors.  $V_d$  and  $N_d$  denote the VIS descriptor and NIR descriptor, respectively.

Feature difference learning and Euclidean distance are essentially measuring difference features and have similarities. They all drive the feature extraction network to extract the differential features of the image patch relative to other image patches. This provides a foundation for building a stable and efficient bridge between descriptor learning and metric learning.

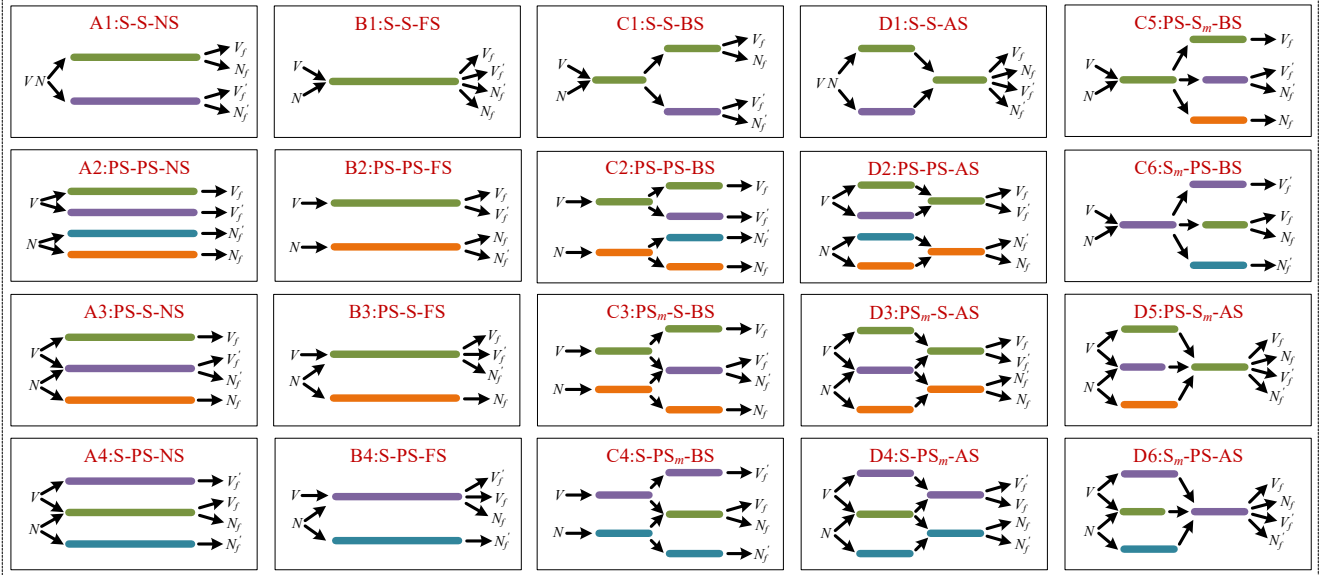


Figure 3. Various combined network architectures of descriptor learning and metric learning. In the subtitle, the three parts divided by short dashes denote the metric network structure, the descriptor network structure, and the parameters sharing between the two. “S” denotes Siamese. “PS” denotes Pseudo-Siamese. “NS” denotes no parameters are shared. “FS” denotes full parameter sharing. “BS” denotes the parameters sharing of the front network layers. “AS” denotes the parameters sharing of the later network layers. In addition, the presence of  $m$  denotes that it is a dominant branch, which makes the structure of the corresponding part of another network consistent with it.

### 3) Feature mapping capabilities of the metric branch.

We find that existing metric learning methods often ignore the feature mapping capability of the metric branch. This is limited by the input data format and network structure characteristics. Existing metric learning methods use uniform and fixed positive and negative sample pairs as inputs. It is difficult to effectively improve the capability of the metric branch without changing its structure. At the same time, adding the network layers to the metric branch would consume more resources with relatively limited performance improvements [14]. The metric branch of the metric network is essentially equivalent to a learnable discriminator. We consider that if we can provide more effective samples for learning, it will theoretically have stronger discriminative performance. However, this is difficult to achieve when using the input data form of existing metric learning methods. Therefore, we break the limitation, only use positive sample pairs in the dataset as inputs and randomly generate negative sample pairs for learning. However, directly generating negative samples often yields mostly simple examples, limiting the effective learning of the metric branch. In addition, unlike the descriptor learning method, the metric branch of the metric learning method combines the features of the two branches and finally outputs a similarity, which results in the inability to directly perform effective hard negative sample mining. Therefore, we attempt to combine descriptor learning to achieve effective knowledge guidance for metric learning, thereby achieving effective hard negative sample mining for metric learning methods.

### 3.2. Overview

To break the performance bottleneck of current research, we break away from the inertial thinking of building a more complex feature relation extraction network structure. From Fig. 2, we break the input format limitation of existing metric learning methods and construct an end-to-end knowledge-guided learning network (KGL-Net), which is the first to realize effective hard negative sample mining for metric learning and establish a stable and efficient bridge between descriptor learning and metric learning. Our KGL-Net has achieved amazing performance advantages while abandoning complex network structures, and it has strong scalability. Specifically, KGL-Net can be divided into three parts: feature extraction network part, hard negative sample mining part and metric branch part. For the feature extraction network part, it includes the feature extraction part of the metric network (light yellow area) and the descriptor network (light purple area). The low-level network layer in the descriptor network is shared with the metric network. In the hard negative sample mining part, a HNSM-M strategy is proposed and used, which uses the descriptors output by the descriptor network to obtain the position index of hard negative samples and guides the features extracted by the metric network. For the metric branch, we apply the feature difference learning [1, 12] and three fully connected layers with 512, 256, and 1 neurons, which can effectively extract the difference features between image patches and perform feature mapping to determine whether the input image patch pairs are matched.

### 3.3. Combined Network Architecture

To ensure the stability and efficiency of the bridge between descriptor learning and metric learning, we explore 20 combined network architectures, including those with no parameters shared (A1-A4), full parameter sharing (B1-B4), parameter sharing of low-level network layers (C1-C6), and parameter sharing of high-level network layers (D1-D6). The C3 architecture is finally selected. In C3 architecture, the metric network is a Pseudo-Siamese structure, the descriptor network is a Siamese structure, and the low-level network layers of the descriptor network become a Pseudo-Siamese structure to achieve the sharing of the low-level network layers of the metric network.

Specifically, paired image patches are first input into two feature extraction branches that do not share parameters to extract their respective low-level detail features. This part has two characteristics. On the one hand, the parameters of different spectral branches are not shared, which is conducive to fully extracting the detailed features of the different spectral image patches. On the other hand, the parameters of the descriptor network and the metric network are shared, which not only helps both to effectively guide the extraction of low-level features, but also provides a basis for subsequent effective knowledge guidance of hard negative samples. Then, the low-level feature maps of the two branches are input into the Pseudo-Siamese metric network, which helps to further fully extract the high-level semantic features of each spectral [14]. At the same time, the low-level feature maps are also input into the Siamese descriptor network to extract high-level semantic features that tend to be in the same feature space [3], which helps to achieve more refined hard negative sample mining, thereby providing more effective knowledge guidance.

### 3.4. HNSM-M strategy

Different from the existing methods, we consider that the feature mapping ability of the metric branch should receive more attention. To improve the discriminative ability of the metric branch with the same structure, a HNSM-M strategy is proposed. From Fig. 2, for the input positive sample pairs, we use the descriptor network to generate descriptors and use the metric network based on feature difference learning to generate high-level feature maps. Benefiting from the sharing of low-level network layers, the constraints of feature-guided loss (see Section 3.5), and the feature extraction consistency, there is a corresponding relation between the descriptors and the high-level feature maps, and they can guide each other's learning.

Taking VIS-NIR as an example, for a training batch containing  $N$  sample pairs, the corresponding positive descriptor pairs  $\{V_{d_i}, N_{d_i}\}_{i=1 \dots N}$  and the corresponding positive high-level feature map pairs  $\{V_{f_i}, N_{f_i}\}_{i=1 \dots N}$  are obtained after passing through the feature extraction part of the descriptor network and the metric network. First, we use

the obtained descriptors to construct the feature distance matrix to traverse and obtain the feature distances of the positive sample pairs and all negative sample pairs:

$$M_{ij} = \left\| N_{d_i} - V_{d_j} \right\|_2 \quad (5)$$

where  $M_{ij}$  denotes the feature distance. Since this operation can be vectorized, the resource consumption of the process is very small.

Second, on the basis of the constructed distance matrix, we can quickly obtain the index position of the VIS descriptor that is most similar to a VIS descriptor in a batch:

$$Index_j = \underset{i}{\operatorname{argmin}} M_{ij} \quad (6)$$

Finally, the index is passed to the output of the high-level feature maps of the metric network to help the VIS feature map quickly find the corresponding NIR feature map and combine them into a hard negative sample pair.

By randomly shuffling the positive high-level feature map pairs and the same number of hard negative high-level feature map pairs and inputting them into the metric branch, the metric branch has better discrimination ability, which also promotes the positive optimization of the feature extraction network.

### 3.5. Loss Function

This work aims to establish a stable and efficient bridge between descriptor learning and metric learning. We find that the feature extraction consistency of the two methods. However, owing to their inherent characteristics, although the high-level feature maps reflect semantic features, the output of the descriptor network tends to reflect global features more, whereas the output of the metric network tends to reflect local features more. To ensure that the hard negative sample positions obtained by the descriptor can have strict guiding significance for the metric network, we construct a feature-guided loss to achieve effective mutual guidance of the high-level feature maps of the two methods:

$$L_{fg}^v = \frac{1}{N} \sum_{i=1}^N \left\| V_{f_i} - V'_{f_i} \right\|_2 \quad (7)$$

$$L_{fg}^n = \frac{1}{N} \sum_{i=1}^N \left\| N_{f_i} - N'_{f_i} \right\|_2 \quad (8)$$

where  $L_{fg}^v$  and  $L_{fg}^n$  denote the feature-guided loss outputs of the VIS branch and the NIR branch, respectively.

In addition to the feature-guided loss, we employ descriptor loss and metric loss to constrain the learning of the descriptor and metric network components in KGL-Net. The descriptor loss is a hybrid similarity measure for triplet margin loss [43], whereas the metric loss uses the conventional binary cross-entropy loss [1]. The total loss is calculated as follows:

$$L = L_d + \alpha L_m + \beta (L_{fg}^v + L_{fg}^n) \quad (9)$$

where  $L$ ,  $L_d$  and  $L_m$  denote the total loss, descriptor loss and

Table 1. Comparison of FPR95 among KGL-Net and nineteen SOTA methods on the VIS-NIR patch dataset.

Models	Field	Forest	Indoor	Mountain	Oldbuilding	Street	Urban	Water	Mean
Traditional methods									
SIFT [20][ICV 04 <sup>*</sup> ]	39.44	11.39	10.13	28.63	19.69	31.14	10.85	40.33	23.95
GISIFT [24][ICIP 11 <sup>*</sup> ]	34.75	16.63	10.63	19.52	12.54	21.80	7.21	25.78	18.60
LGHD [29][ICIP 15 <sup>*</sup> ]	16.52	3.78	7.91	10.66	7.91	6.55	7.21	12.76	9.16
Descriptor learning									
PN-Net [33][arXiv 16 <sup>*</sup> ]	20.09	3.27	6.36	11.53	5.19	5.62	3.31	10.72	8.26
Q-Net [35][Sensors 17 <sup>*</sup> ]	17.01	2.70	6.16	9.61	4.61	3.99	2.83	8.44	6.91
L2-Net [41][CVPR 17 <sup>*</sup> ]	13.67	2.48	4.63	8.87	4.12	5.58	1.54	6.55	5.93
HardNet [37][NeurIPS 17 <sup>*</sup> ]	5.61	0.15	1.50	3.14	1.10	1.93	0.69	2.29	2.05
SOSNet [42][CVPR 19 <sup>*</sup> ]	5.94	0.13	1.53	2.45	0.99	2.04	0.78	1.90	1.97
HyNet [43][NeurIPS 20 <sup>*</sup> ]	4.50	0.07	1.09	1.80	0.83	0.52	0.53	1.91	1.41
Metric learning									
Siamese [10][CVPRW 16 <sup>*</sup> ]	15.79	10.76	11.60	11.15	5.27	7.51	4.60	10.21	9.61
Pseudo-Siamese [10][CVPRW 16 <sup>*</sup> ]	17.01	9.82	11.17	11.86	6.75	8.25	5.65	12.04	10.31
2-channe [10][CVPRW 16 <sup>*</sup> ]	9.96	0.12	4.40	8.89	2.30	2.18	1.58	6.40	4.47
SCFDM [47][ACCV 18 <sup>*</sup> ]	7.91	0.87	3.93	5.07	2.27	2.22	0.85	4.75	3.48
MR_3A [46][TIP 21 <sup>*</sup> ]	4.21	0.11	1.12	0.87	0.67	0.56	0.43	1.90	1.23
AFD-Net [12, 13][ICCV 19 <sup>*</sup> , TNNLS 21 <sup>*</sup> ]	3.47	0.08	1.48	<u>0.68</u>	0.71	0.42	0.29	1.48	1.08
SPIMNet [49][Inf. Fusion 23 <sup>*</sup> ]	<u>2.28</u>	0.09	1.62	0.88	0.69	0.29	0.42	2.26	1.07
EFR-Net [15][TGRS 23 <sup>*</sup> ]	2.84	0.07	1.09	0.79	0.61	0.50	0.34	1.65	0.99
MFD-Net [14][TGRS 22 <sup>*</sup> ]	2.59	<b>0.02</b>	1.24	0.95	<u>0.48</u>	<u>0.24</u>	<u>0.12</u>	<u>1.44</u>	0.88
FIL-Net [1][TIP 23 <sup>*</sup> ]	2.61	0.04	0.98	0.73	0.49	0.34	<b>0.10</b>	1.49	<u>0.85</u>
<b>KGL-Net (Ours)</b>	<b>1.00</b>	<u>0.03</u>	<b>0.83</b>	<b>0.28</b>	<b>0.47</b>	<b>0.20</b>	0.17	<b>1.37</b>	<b>0.54</b>

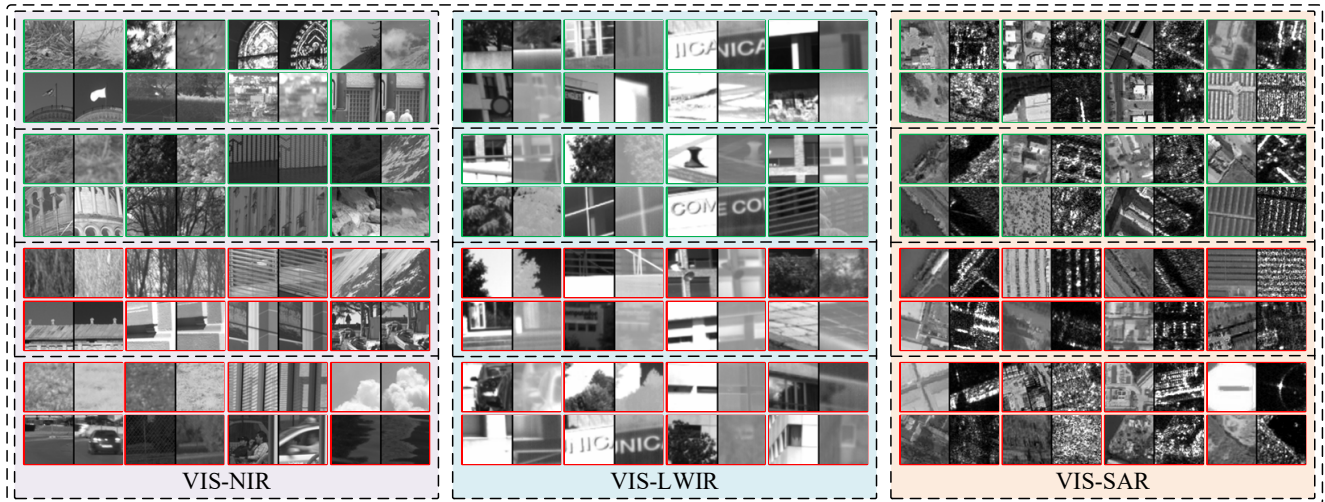


Figure 4. The matching effect of KGL-Net on the VIS-NIR patch dataset (VIS-NIR), VIS-LWIR patch dataset (VIS-LWIR) and OS patch dataset (VIS-SAR). Each cross-spectral scene is from top to bottom: correctly judged as matching, correctly judged as non-matching, misjudged as matching, and misjudged as non-matching. Green denotes a correct judgment, and red denotes an incorrect judgment.

metric loss, respectively. The detailed descriptor loss details can be found in [43]. Both  $\alpha$  and  $\beta$  are set to 1.

## 4. Experiments

### 4.1. Datasets

Three public datasets of different cross-spectral scenarios are experimented, including the VIS-NIR patch dataset [10, 50], the VIS-LWIR patch dataset [1, 10] and

the OS patch dataset [15, 51]. The VIS-NIR patch dataset is a VIS and NIR image patch matching dataset that contains more than 1.6 million sample pairs and is divided into 9 subsets. Consistent with previous studies, the ‘‘Country’’ subset is used for training, and the other 8 subsets are used for testing. The VIS-LWIR patch dataset is a VIS and long-wave infrared (LWIR) image patch matching dataset that includes 21370 sample pairs. We divide it according to [1]. The OS patch dataset is a VIS and synthetic aperture radar (SAR) image patch matching dataset that includes

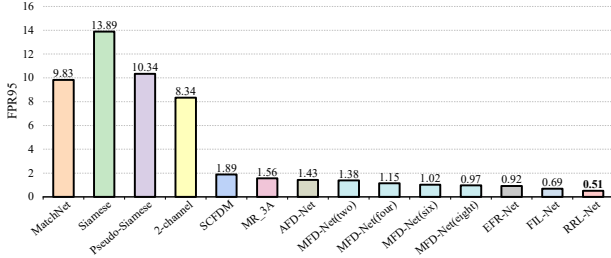


Figure 5. FPR95 comparison of multiple excellent methods on the VIS-LWIR patch dataset.

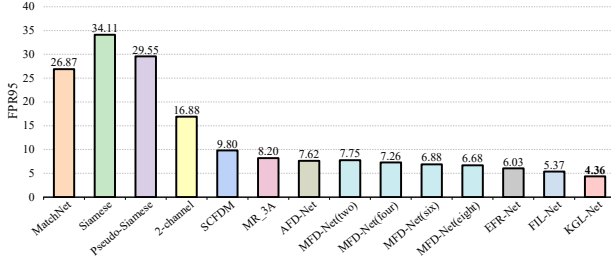


Figure 6. FPR95 comparison of multiple excellent methods on the OS patch dataset.

123676 sample pairs. We divide it according to [15]. Compared with VIS-NIR and VIS-LWIR, VIS-SAR has significantly severe nonlinear differences. The image patch size of all three datasets is  $64 \times 64$  pixels. Notably, only positive samples in the training set are used as our input.

## 4.2. Experimental Details

In the experiment, the batch size is 256, and the GPU is RTX 3090 24G. To ensure that the network can fully learn hard samples, the training epochs on the VIS-NIR patch dataset and VIS-LWIR patch dataset is 100, and the training epochs on the OS patch dataset is 200. Consistent with [37, 41-43], the descriptor length is 128. In addition, instead of using a single learning rate, we use a learning rate of  $5e^{-3}$  for the feature extraction part and  $5e^{-5}$  for the metric branch and use the Adam [52] optimizer to train the model. For the evaluation metric, consistent with existing studies [1-3, 10, 12-15, 31-49], the false positive rate at 95% recall (FPR95) is used. The smaller the FPR95, the better. Bold denotes the optimal result, and underline denotes the suboptimal result.

## 4.3. Comparison with SOTA Methods

We conduct a detailed comparison of our KGL-Net with various excellent image patch matching methods in three different cross-spectral scenarios (VIS-NIR, VIS-LWIR and VIS-SAR). More experimental results are provided in the Supplementary Materials.

**1) VIS-NIR image matching.** From the results of “Mean” in Table 1, our KGL-Net achieves the best results. Compared with MFD-Net, the latest FIL-Net reduces the FPR95 by only 3.4% (from 0.88 to 0.85). However,

compared with the latest FIL-Net, KGL-Net has fewer parameters and reduces the FPR95 by 36.5% (from 0.85 to 0.54). The performance improvement is enormous and breaks the existing inherent thinking that focuses on mining feature relations between image patches. From the results of each subset, our KGL-Net achieves the best results on six subsets. The most significant improvement is achieved on the “Field” subset, which is identified as the most difficult subset of the dataset. This fully verifies that realizing hard negative sample mining for metric learning will effectively promote its correct discrimination of hard samples. In addition, from the results of “VIS-NIR” in Fig. 4, most of the misjudged samples fall into two categories. On the one hand, owing to the spatiotemporal differences in the data acquisition, partially moving objects can cause image pairs to be marked as matching but visually non-matching. On the other hand, some non-matching image pairs with adjacent coordinates have extremely similar semantic features. In addition, from the correct sample pairs, our KGL-Net has an excellent matching effect in overcoming the spectral difference between VIS and NIR.

**2) VIS-LWIR image matching.** As presented in Fig. 5, compared with other excellent methods, our KGL-Net can reduce the FPR95 by 26.1% (from 0.69 to 0.51) - 96.3% (from 13.89 to 0.51). The improvement of KGL-Net is very significant. From Fig. 4, compared with VIS-NIR, the pixel-level nonlinear difference in VIS-LWIR is more obvious. These results further verify that KGL-Net has excellent robustness in VIS-LWIR cross-spectral scenarios and datasets with a small number of samples.

**3) VIS-SAR image matching.** From Fig. 6, compared with other excellent methods, our KGL-Net can reduce FPR95 by 18.8% (from 5.37 to 4.36) - 87.2% (from 34.11 to 4.36), which verifies the excellent performance of our KGL-Net in VIS-SAR. From Fig. 4, compared with VIS-NIR and VIS-LWIR, the VIS-SAR cross-spectral scenario has significantly more serious pixel-level nonlinear differences, which directly leads to the occurrence of misjudgments. However, it can be found from the correct sample pairs that KGL-Net also has good robustness in VIS-SAR cross-spectral scenarios.

## 4.4. Ablation Experiment

**1) Break-down ablation.** To further verify the proposed components, we conduct detailed ablation experiments in Table 2. Compared with the single metric network, the FPR95 decreases by 12.5% (from 0.88 to 0.77), 35.2% (from 0.88 to 0.57), and 38.6% (from 0.88 to 0.57) when CNA, HNSM-N, and FGL are added one by one. Among them, using our HNSM-M strategy to mine hard negative samples for learning results in the most significant improvement. Specifically, compared with using only the CNA, the additional use of HNSM-M strategy resulted in a 26.0% (from 0.77 to 0.57) decrease in FPR95. This is an amazing improvement without increasing the parameters.

Table 2. Break-down ablation experiments on the VIS-NIR patch dataset. *CNA* denotes the combined network architecture. *FGL* denotes feature-guided loss. *w/o all* refers to using only the metric network with a Pseudo-Siamese structure.

Methods	Variants			FPR95 ↓
	CNA	HNSM-M	FGL	
Our-w/o all	✗	✗	✗	0.88 (-38.6%)
Our-w/ CNA	✓	✗	✗	0.77 (-29.9%)
Our-w/ CNA and HNSM-M	✓	✓	✗	0.57 (-5.3%)
KGL-Net (Ours)	✓	✓	✓	<b>0.54</b>

Table 3. Comparison of different combined network architectures on the VIS-NIR patch dataset. The results with background color denote the results obtained via the HNSM-M strategy.

CNA	FPR95 ↓	CNA	FPR95 ↓	CNA	FPR95 ↓	CNA	FPR95 ↓
A1	1.09 (-33.0%)	A2	0.98 (-6.1%)	A3	0.84 (-20.2%)	A4	0.96 (-26.0%)
	<b>0.73</b>		<b>0.92</b>		<b>0.67</b>		<b>0.71</b>
B1	1.07 (-6.5%)	B2	1.44 (-20.1%)	B3	1.02 (-19.6%)	B4	1.22 (-16.4%)
	<b>1.00</b>		<b>1.15</b>		<b>0.82</b>		<b>1.02</b>
C1	0.93 (-35.5%)	C2	0.98 (-37.8%)	C3	0.81 (-33.3%)	C4	1.02 (-37.3%)
	<b>0.60</b>		<b>0.61</b>		<b>0.54</b>		<b>0.64</b>
D1	1.49 (-35.6%)	D2	1.75 (-38.9%)	D3	1.52 (-39.5%)	D4	1.34 (-17.9%)
	<b>0.96</b>		<b>1.07</b>		<b>0.92</b>		<b>1.10</b>
C5	0.88 (-31.8%)	C6	0.97 (-25.8%)	D5	1.24 (-21.0%)	D6	1.28 (-30.5%)
	<b>0.60</b>		<b>0.72</b>		<b>0.98</b>		<b>0.89</b>

Table 4. Comparison of different network layer sharing based on the C3 architecture on the VIS-NIR patch dataset. Sharing layer addition rules are added sequentially from the low to the high.

Shared layers	FPR95 ↓	Shared layers	FPR95 ↓	Shared layers	FPR95 ↓
0	0.67	3	0.54	6	0.65
1	0.59	4	<b>0.54</b>	7	0.75
2	0.58	5	0.59	8	0.93

Table 5. Comparison of KGL-Net with different learning rates on the VIS-NIR patch dataset. The left and right sides of the “/” denotes the learning rates of the feature extraction part and the metric branch part. “-” denotes the training collapse.

learning rates	FPR95 ↓	learning rates	FPR95 ↓	learning rates	FPR95 ↓	learning rates	FPR95 ↓
5e <sup>-2</sup> /5e <sup>-3</sup>	-	5e <sup>-3</sup> /5e <sup>-3</sup>	-	5e <sup>-4</sup> /5e <sup>-3</sup>	-	5e <sup>-3</sup> /5e <sup>-3</sup>	-
5e <sup>-2</sup> /5e <sup>-4</sup>	-	5e <sup>-3</sup> /5e <sup>-4</sup>	-	5e <sup>-4</sup> /5e <sup>-4</sup>	-	5e <sup>-4</sup> /5e <sup>-5</sup>	-
5e <sup>-2</sup> /5e <sup>-5</sup>	0.72	5e <sup>-3</sup> /5e <sup>-5</sup>	<b>0.54</b>	5e <sup>-4</sup> /5e <sup>-5</sup>	0.60	5e <sup>-5</sup> /5e <sup>-5</sup>	0.92
5e <sup>-2</sup> /5e <sup>-6</sup>	0.90	5e <sup>-3</sup> /5e <sup>-6</sup>	0.66	5e <sup>-4</sup> /5e <sup>-6</sup>	0.68	5e <sup>-5</sup> /5e <sup>-6</sup>	1.13

**2) Combined network architecture.** We conduct detailed experimental research on 20 combined network architectures. From Table 3, the construction of the combined network architecture has a significant impact. The B and D series have poor overall performance, whereas the A and C series have good overall performance. Owing to their own characteristics, compared with the metric network, the final output features of the feature extraction network part of the descriptor network focus more on global features. Directly sharing parameters between the two methods (B series) or the parameters of the latter network layers (D series) will cause the network to be overly constrained in the initial training stage, resulting in learning confusion and performance degradation. At the same time, compared with the A series, the C series has better performance. This show that the two methods sharing

low-level network layers can help each other to extract richer detailed features. It also further verifies that the descriptor network and the metric network need to establish appropriate connections. In addition, we find that when the descriptor network is a Siamese structure and the metric network is a Pseudo-Siamese structure (A3, B3, C3, D3), it has almost the best result in the same series. These can provide the experience for the subsequent design of bridges. Moreover, when the same combined network architecture is used, the FPR95 decreases by 6.5%-39.5% when using the HNSM-M strategy compared to not using it. This fully verifies the superiority of our HNSM-M strategy.

**3) Number of shared network layers.** We explore various sharing schemes on the C3 architecture. From Table 4, when the number of shared layers continues to increase, FPR95 first decreases and then increases. This further proves that reasonably shared low-level network layers are effective. Compared with not sharing and sharing 8 layers, sharing the first 4 layers will reduce FPR95 by 19.4% (from 0.67 to 0.54) and 41.9% (from 0.93 to 0.54).

#### 4.5. Discuss of “Learning rate”

Unlike the direct single learning rate setting, we use different learning rates for the feature extraction part and metric branch part of the network. From Table 5, when the learning rate of the metric branch is set too high, KGL-Net will collapse. Meanwhile, compared with the final use of “5e<sup>-3</sup>/5e<sup>-5</sup>”, when the learning rates of the two parts are consistent (5e<sup>-5</sup>/5e<sup>-5</sup>), the matching performance decreases significantly. The feature extraction part needs a larger learning rate, whereas the metric branch part should be smaller. On the one hand, the metric branch is relatively simple compared with the feature extraction network. On the other hand, the metric branch will further handle hard negative sample pairs.

## 5. Conclusion

For the performance bottleneck of current research, we break away from the inertial thinking of building a more complex feature relation extraction network structure and make the first attempt to explore a stable and efficient bridge between descriptor learning and metric learning. On the basis of the discovered feature extraction consistency, we construct an efficient KGL-Net, which realizes the mining of hard negative samples for metric learning for the first time. Our KGL-Net achieves amazing performance improvements while abandoning complex network structures. At the same time, we also conduct a detailed exploration of 20 basic combined network architectures, which provide reference experience for the bridge design between the two methods. We hope that our interesting findings and new research ideas can inspire researchers to rethink the feasibility and superiority of combined learning methods in cross-spectral image patch matching tasks.



## References

- [1] Chuang Yu, Yunpeng Liu, Jinmiao Zhao, Shuhang Wu, and Zhuhua Hu. Feature Interaction Learning Network for Cross-Spectral Image Patch Matching. *IEEE Transactions on Image Processing*, 32: 5564-5579, 2023. 1, 2, 3, 4, 5, 6, 7
- [2] Dou Quan, Shuang Wang, Yu Gu, Ruiqi Lei, Bowu Yang, Shaowei Wei, Biao Hou, and Licheng Jiao. Deep Feature Correlation Learning for Multi-Modal Remote Sensing Image Registration. *IEEE Transactions on Geoscience and Remote Sensing*, 60: 1-16, 2022. 1, 7
- [3] Dou Quan, Huiyuan Wei, Shuang Wang, Ruiqi Lei, Baorui Duan, Yi Li, Biao Hou, and Licheng Jiao. Self-Distillation Feature Learning Network for Optical and SAR Image Registration. *IEEE Transactions on Geoscience and Remote Sensing*, 60: 1-18, 2022. 1, 7
- [4] Fengyin Lin, Mingkang Li, Da Li, Timothy Hospedales, Yi-Zhe Song, and Yonggang Qi. Zero-Shot Everything Sketch-Based Image Retrieval, and in Explainable Style. In *Proceedings of the IEEE Conference on Computer Vision and Pattern Recognition (CVPR)*, pages 23349-23358, 2023. 1
- [5] Vassileios Balntas, Karel Lenc, Andrea Vedaldi, Tinne Tuytelaars, Jiri Matas, and Krystian Mikolajczyk. H-Patches: A Benchmark and Evaluation of Handcrafted and Learned Local Descriptors. *IEEE Transactions on Pattern Analysis and Machine Intelligence*, 42(11): 2825-2841, 2020. 1
- [6] Yujiao Shi and Hongdong Li. Beyond Cross-view Image Retrieval: Highly Accurate Vehicle Localization Using Satellite Image. In *Proceedings of the IEEE Conference on Computer Vision and Pattern Recognition (CVPR)*, pages 16989-16999, 2022. 1
- [7] Yicheng Wang, Zhenzhong Chen, Feng Wu, and Gang Wang. Person re-identification with cascaded pairwise convolutions. In *Proceedings of the IEEE Conference on Computer Vision and Pattern Recognition (CVPR)*, pages 1470-1478, 2018. 1
- [8] Cuiqun Chen, Mang Ye, Meibin Qi, Jingjing Wu, Jianguo Jiang, and Chia-Wen Lin. Structure-Aware Positional Transformer for Visible-Infrared Person Re-Identification. *IEEE Transactions on Image Processing*, 31: 2352-2364, 2022. 1
- [9] Qize Yang, Hong-Xing Yu, Ancong Wu, and Wei-Shi Zheng. Patch-Based Discriminative Feature Learning for Unsupervised Person Re-Identification. In *Proceedings of the IEEE Conference on Computer Vision and Pattern Recognition (CVPR)*, pages 3628-3637, 2019. 1
- [10] Cristhian A. Aguilera, Francisco J. Aguilera, Angel D. Sappa, Cristhian Aguilera, and Ricardo Toledo. Learning Cross-Spectral Similarity Measures with Deep Convolutional Neural Networks. In *Proceedings of the IEEE Conference on Computer Vision and Pattern Recognition Workshops (CVPRW)*, pages 267-275, 2016. 1, 2, 6, 7
- [11] Nati Ofir, Shai Silberstein, Hila Levi, Dani Rozenbaum, Yosi Keller, and Sharon Duvdevani Bar. Deep multi-spectral registration using invariant descriptor learning. In *Proceedings of the IEEE International Conference on Image Processing (ICIP)*, pages 1238-1242, 2018. 1, 6
- [12] Dou Quan, Xuefeng Liang, Shuang Wang, Shaowei Wei, Yanfeng Li, Ning Huyan, and Licheng Jiao. AFD-Net: Aggregated feature difference learning for cross-spectral image patch matching. In *Proceedings of the IEEE International Conference on Computer Vision (ICCV)*, pages 3017-3026, 2019. 1, 2, 3, 4, 6, 7
- [13] Dou Quan, Shuang Wang, Ning Huyan, Jocelyn Chanussot, Ruoqing Wang, Xuefeng Liang, Biao Hou, and Licheng Jiao. Element-Wise Feature Relation Learning Network for Cross-Spectral Image Patch Matching. *IEEE Transactions on Neural Networks and Learning Systems*, 33(8): 3372-3386, 2021. 1, 2, 3, 6, 7
- [14] Chuang Yu, Yunpeng Liu, Chenxi Li, Lin Qi, Xin Xia, Tianci Liu, and Zhuhua Hu. Multibranch Feature Difference Learning Network for Cross-Spectral Image Patch Matching. *IEEE Transactions on Geoscience and Remote Sensing*, 60: 1-15, 2022. 1, 2, 3, 4, 5, 6, 7
- [15] Chuang Yu, Jinmiao Zhao, Yunpeng Liu, Shuhang Wu, and Chenxi Li. Efficient Feature Relation Learning Network for Cross-Spectral Image Patch Matching. *IEEE Transactions on Geoscience and Remote Sensing*, 61: 1-17, 2023. 1, 2, 3, 6, 7
- [16] Daniel I. Barnea and Harvey F. Silverman. A class of algorithms for fast digital image registration. *IEEE Transactions on Computers*, C-21(2):179-186, 1972. 1
- [17] Azriel Rosenfeld and Gordon J. Vanderbrug. Coarse-fine template matching. *IEEE Transactions on Systems, Man, and Cybernetics*, 7(2): 104-107, 1977. 1
- [18] Gordon J. Vanderbrug and Azriel Rosenfeld. Two-stage template matching. *IEEE Transactions on Computers*, C-26(4): 384-393, 1977. 1
- [19] Paul Viola and William M. Wells. Alignment by maximization of mutual information. In *Proceedings of the IEEE International Conference on Computer Vision (ICCV)*, pages 16-23, 1995. 1
- [20] David G. Lowe. Distinctive image features from scale-invariant keypoints. *International Journal of Computer Vision*. 60(2): 91-110, 2004. 1, 6
- [21] Navneet Dalal and Bill Triggs. Histograms of oriented gradients for human detection. In *Proceedings of the IEEE Conference on Computer Vision and Pattern Recognition (CVPR)*, pages 886-893, 2005. 1
- [22] Herbert Bay, Andreas Ess, Tinne Tuytelaars, and Luc Van Gool. Speeded-up robust features (SURF). *Computer Vision And Image Understanding*, 110(3): 346-359, 2008. 1
- [23] Ethan Rublee, Vincent Rabaud, Kurt Konolige, and Gary Bradski. ORB: An efficient alternative to SIFT or SURF. In *Proceedings of the IEEE International Conference on Computer Vision (ICCV)*, pages 2564 -2571, 2011. 1
- [24] Damien Firmenichy, Matthew Brown, and Sabine Süsstrunk. Multispectral interest points for RGB-NIR image registration. In *Proceedings of the IEEE International Conference on Image Processing (ICIP)*, pages 181-184, 2011. 1, 6
- [25] Peter pinggera, Toby Breckon, and Horst Bischof. On cross-spectral stereo matching using dense gradient features. In *Proceedings of the British Machine Vision Conference (BMVC)*, 2012. 1
- [26] Cristhian Aguilera, Fernando Barrera, Felipe Lumbreras, Angel D. Sappa, and Ricardo Toledo. Multispectral image feature points. *Sensors*, 12(9): 12661-12672, 2012. 1
- [27] Pablo Fernandez Alcantarilla, Adrien Bartoli, and Andrew J. Davison. Kaze features, In *Proceedings of the European Conference on Computer Vision (ECCV)*, pages 214-227, 2012. 1
- [28] Tarek Mouats, Nabil Aouf, Angel Domingo Sappa, Cristhian Aguilera, and Ricardo Toledo. Multispectral stereo odometry.

- IEEE Transactions on Intelligent Transportation Systems*, 16(3): 1210-1224, 2015. 1
- [29] Cristhian A. Aguilera, Angel D. Sappa, and Ricardo Toledo. LGHD: A feature descriptor for matching across non-linear intensity variations. In *Proceedings of the IEEE International Conference on Image Processing (ICIP)*, pages 178-181, 2015. 1, 6
- [30] Yann LeCun, Yoshua Bengio, and Geoffrey Hinton. Deep learning. *Nature*, 521: 436-444, 2015. 1
- [31] Edgar Simo-Serra, Eduard Trulls, Luis Ferraz, Iasonas Kokkinos, Pascal Fua, and Francesc Moreno-Noguer. Discriminative learning of deep convolutional feature point descriptors. In *Proceedings of the IEEE International Conference on Computer Vision (ICCV)*, pages 118-126, 2015. 1, 2, 7
- [32] Vassileios Balntas, Edgar Riba, Daniel Ponsa, and Krystian Mikolajczyk. Learning local feature descriptors with triplets and shallow convolutional neural networks. In *Proceedings of the British Machine Vision Conference (BMVC)*, pages 119.1-119.11, 2016. 1, 2, 7
- [33] Vassileios Balntas, Edward Johns, Lilian Tang, and Krystian Mikolajczyk. PN-Net: Conjoined Triple Deep Network for Learning Local Image Descriptors. *arXiv preprint arXiv:1601.05030*, 2016. 1, 2, 6, 7
- [34] B G Vijay Kumar, Gustavo Carneiro, and Ian Reid. Learning Local Image Descriptors with Deep Siamese and Triplet Convolutional Networks by Minimizing Global Loss Functions. In *Proceedings of the IEEE Conference on Computer Vision and Pattern Recognition (CVPR)*, pages 5385-5394, 2016. 1, 2, 7
- [35] Cristhian A. Aguilera, Angel D. Sappa, Cristhian Aguilera, and Ricardo Toledo. Cross-Spectral Local Descriptors via Quadruplet Network. *Sensors*, 17(4), 2017. 1, 2, 6, 7
- [36] Xu Zhang, Felix X. Yu, Sanjiv Kumar, and Shih-Fu Chang. Learning Spread-Out Local Feature Descriptors. In *Proceedings of the IEEE International Conference on Computer Vision (ICCV)*, pages 4605-4613, 2017. 1, 2, 7
- [37] Anastasiya Mishchuk, Dmytro Mishkin, Filip Radenović, and Jiri Matas. Working hard to know your neighbor's margins: Local descriptor learning loss. In *Proceedings of the Advances in Neural Information Processing Systems (NeurIPS)*, pages 4827-4838, 2017. 1, 2, 6, 7
- [38] Chong Wang, Xipeng Lan, and Xue Zhang. How to train triplet networks with 100K identities. In *Proceedings of the IEEE International Conference on Computer Vision Workshops (ICCVW)*, 1907-1915, 2017. 1, 2, 7
- [39] Wenzhao Zheng, Zhaodong Chen, Jiwen Lu, and Jie Zhou. Hardness-aware deep metric learning. In *Proceedings of the IEEE Conference on Computer Vision and Pattern Recognition (CVPR)*, pages 72-81, 2019. 1, 2, 7
- [40] Shuang Wang, Yanfeng Li, Xuefeng Liang, Dou Quan, Bowu Yang, Shaowei Wei, and Licheng Jiao. Better and Faster: Exponential Loss for Image Patch Matching. In *Proceedings of the IEEE International Conference on Computer Vision (ICCV)*, pages 4811-4820, 2019. 1, 2, 7
- [41] Yurun Tian, Bin Fan, and Fuchao Wu. L2-Net: Deep learning of discriminative patch descriptor in Euclidean space. In *Proceedings of the IEEE Conference on Computer Vision and Pattern Recognition (CVPR)*, pages 661-669, 2017. 1, 2, 6, 7
- [42] Yurun Tian, Xin Yu, Bin Fan, Fuchao Wu, Huub Heijnen, and Vassileios Balntas. SOSNet: Second order similarity regularization for local descriptor learning. In *Proceedings of the IEEE Conference on Computer Vision and Pattern Recognition (CVPR)*, pages 11008-11017, 2019. 1, 2, 6, 7
- [43] Yurun Tian, Axel Barroso-Laguna, Tony Ng, Vassileios Balntas, and Krystian Mikolajczyk. HyNet: Learning local descriptor with hybrid similarity measure and triplet loss. In *Proceedings of the Advances in Neural Information Processing Systems (NeurIPS)*, pages 1-12, 2020. 1, 2, 5, 6, 7
- [44] Xufeng Han, Thomas Leung, Yangqing Jia, Rahul Sukthankar, and Alexander C. Berg. MatchNet: Unifying feature and metric learning for patch-based matching. In *Proceedings of the IEEE Conference on Computer Vision and Pattern Recognition (CVPR)*, pages 3279-3286, 2015. 1, 2, 7
- [45] Sergey Zagoruyko and Nikos Komodakis. Learning to compare image patches via convolutional neural networks. In *Proceedings of the IEEE Conference on Computer Vision and Pattern Recognition (CVPR)*, pages 4353-4361, 2015. 1, 2, 7
- [46] Dou Quan, Shuang Wang, Yi Li, Bowu Yang, Ning Huyan, Jocelyn Chanussot, Biao Hou, and Licheng Jiao. Multi-Relation Attention Network for Image Patch Matching. *IEEE Transactions on Image Processing*, 30: 7127-7142, 2021. 1, 2, 6, 7
- [47] Dou Quan, Shuai Fang, Xuefeng Liang, Shuang Wang, and Licheng Jiao. Cross-spectral image patch matching by learning features of the spatially connected patches in a shared space. In *Proceedings of the Asian Conference on Computer Vision (ACCV)*, pages 115-130, 2018. 1, 2, 3, 6, 7
- [48] Sovann En, Alexis Lechervy, and Frédéric Jurie. TS-NET: Combining modality specific and common features for multimodal patch matching. In *Proceedings of the IEEE International Conference on Image Processing (ICIP)*, pages 3024-3028, 2018. 1, 2, 3, 7
- [49] Yeongmin Ko, Yong-jun Jang, Vinh Quang Dinh, Hae-Gon Jeon, and Moongu Jeon. Spectral-invariant matching network. *Information Fusion*, 91: 623-632, 2023. 1, 2, 3, 6, 7
- [50] Matthew Brown and Sabine Süsstrunk. Multi-spectral SIFT for scene category recognition. In *Proceedings of the IEEE Conference on Computer Vision and Pattern Recognition (CVPR)*, pages 177-184, 2011. 6
- [51] Yuming Xiang, Rongshu Tao, Feng Wang, Hongjian You, and Bing Han. Automatic registration of optical and SAR images via improved phase congruency model. *IEEE Journal of Selected Topics in Applied Earth Observations and Remote Sensing*, 13: 5847-5861, 2020. 6
- [52] Diederik P. Kingma, and Jimmy Lei Ba. Adam: A method for stochastic optimization. In *Proceedings of the International Conference on Learning Representations (ICLR)*, 2015. 7
- [53] Saurabh Singh and Shankar Krishnan. Filter Response Normalization Layer: Eliminating Batch Dependence in the Training of Deep Neural Networks. In *Proceedings of the IEEE Conference on Computer Vision and Pattern Recognition (CVPR)*, pages 11234-11243, 2020. 3
- [54] Qilong Wang, Banggu Wu, Pengfei Zhu, Peihua Li, Wangmeng Zuo, and Qinghua Hu. ECA-Net: Efficient Channel Attention for Deep Convolutional Neural Networks. In *Proceedings of the IEEE Conference on Computer Vision and Pattern Recognition (CVPR)*, pages 11531-11539, 2020. 3

# Why and How: Knowledge-Guided Learning for Cross-Spectral Image Patch Matching

## Supplementary Material



Figure 1. Some samples from the VIS-NIR patch dataset. From left to right, each column is from the “Country”, “Field”, “Forest”, “Indoor”, “Mountain”, “Oldbuilding”, “Street”, “Urban”, and “Water” subsets. Green denotes matching samples, and red denotes non-matching samples. For each image pair, the left is the visible spectrum (VIS), and the right is the near-infrared (NIR).



Figure 2. Some samples from the VIS-LWIR patch dataset. Green denotes matching samples and red denotes non-matching samples. For each image pair, the left is the VIS, and the right is the long-wave infrared (LWIR).

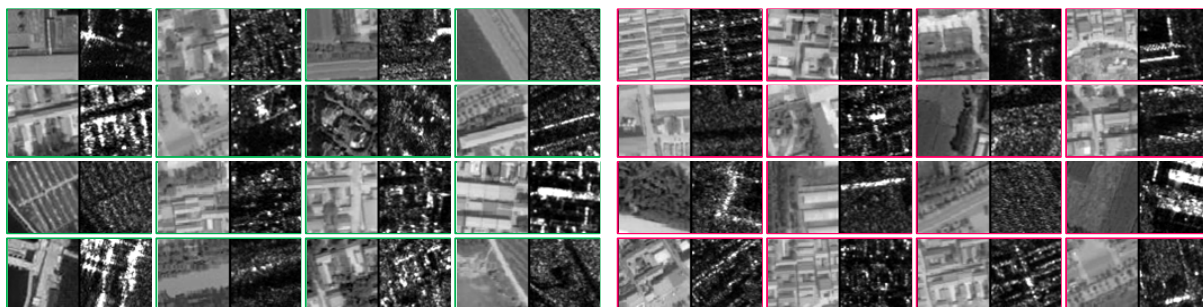


Figure 3. Some samples from the OS patch dataset. Green denotes matching samples and red denotes non-matching samples. For each image pair, the left is the VIS, and the right is the synthetic aperture radar (SAR).

In this supplementary material, we offer extra details and additional results to complement the main paper. In Section A, we offer a more detailed introduction and some sample presentations of three different and public cross-spectral image patch matching datasets (VIS-NIR patch dataset [1, 2], VIS-LWIR patch dataset [3], and OS patch dataset [4, 5]) used in the main paper. In Section B, we offer more additional experimental results to fully explore the

effectiveness of our KGL-Net. In Section C, we provide more discussion on the design of the bridge between descriptor learning and metric learning as well as future research.

### A. Detailed Dataset Introduction

1) *VIS-NIR patch dataset*. It is a VIS-NIR image patch

Table 1. ECA module investigation on the three different cross-spectral scene datasets.

Scheme	VIS-NIR	VIS-LWIR	VIS-SAR
KGL-Net w/o ECA	0.58 (-6.9%)	0.55 (-7.3%)	4.61 (-5.4%)
KGL-Net	<b>0.54</b>	<b>0.51</b>	<b>4.36</b>

Table 2. Investigation of feature difference learning in the metric branch on the VIS-NIR patch dataset.

Scheme	FPR95 ↓
Feature product learning	0.68 (-20.6%)
Feature concatenation learning	0.65 (-16.9%)
Feature difference learning	<b>0.54</b>

Table 3. Learning rate optimization strategy investigation on the VIS-NIR patch dataset. “--” means that no learning rate optimization strategy is used

Strategy	--	Cosine annealing	Simulated annealing
FPR95 ↓	0.54	<b>0.51</b>	0.53

Table 4. Descriptor length investigation on the VIS-NIR patch dataset.

Descriptor length	64	128	256
FPR95 ↓	0.57	0.54	<b>0.53</b>

Table 5. Comparison of different combined network architectures on the VIS-LWIR patch dataset. The results with background color denote the results obtained via the HNSM-M strategy.

CNA	FPR95 ↓	CNA	FPR95 ↓	CNA	FPR95 ↓	CNA	FPR95 ↓
A1	1.94 (-11.9%)	A2	2.45 (-9.4%)	A3	2.35 (-3.8%)	A4	1.80 (-30.6%)
	<b>1.71</b>		<b>2.22</b>		<b>2.26</b>		<b>1.25</b>
B1	1.75 (-36.6%)	B2	1.71 (-29.8%)	B3	1.38 (-43.5%)	B4	1.71 (-38.0%)
	<b>1.11</b>		<b>1.20</b>		<b>0.78</b>		<b>1.06</b>
C1	1.38 (-43.5%)	C2	1.11 (-50.5%)	C3	1.02 (-50.0%)	C4	1.29 (-54.3%)
	<b>0.78</b>		<b>0.55</b>		<b>0.51</b>		<b>0.59</b>
D1	1.89 (-12.2%)	D2	2.81 (-6.4%)	D3	2.22 (-55.9%)	D4	2.49 (-48.2%)
	<b>1.66</b>		<b>2.63</b>		<b>0.98</b>		<b>1.29</b>
E1	1.11 (-41.4%)	E2	1.43 (-45.5%)	E3	2.72 (-52.6%)	E4	2.72 (-49.3%)
	<b>0.65</b>		<b>0.78</b>		<b>1.29</b>		<b>1.38</b>

matching dataset created by Aguilera et al. based on the public VIS-NIR scene dataset [1]. The VIS-NIR patch dataset is widely used to evaluate the performance of cross-spectral image patch matching methods. The dataset is created by first obtaining VIS image patches via the SIFT [6] keypoint extraction method and then cropping them around these keypoints. Then, half of the VIS image patches and the NIR image patches with the same keypoint coordinates are combined into matching sample pairs (positive samples). Finally, the other half of the VIS image patches are combined with randomly selected NIR image patches to form non-matching sample pairs (negative samples). It contains 9 subsets with a total of more than 1.6 million pairs with equal positive and negative samples, namely, Country (277,504), Field (240,896), Forest (376,832), Indoor (60,672), Mountain (151,296), Oldbuilding (101,376), Street (164,608), Urban (147,712) and Water (143,104). Fig. 1 shows some samples from the

dataset, where the size of each image patch is 64×64 pixels. To fairly verify the performance of the proposed method, consistent with previous studies [2, 3, 5, 7-12], the “Country” subset is used for training, and the remaining 8 subsets are used for testing.

2) *VIS-LWIR patch dataset*. It is based on 44 registered pairs of VIS and LWIR images acquired from the campus of the Autonomous University of Barcelona. The resolution of the collected original images is 639×431 pixels. Different from the construction method of the VIS-NIR patch dataset, the VIS-LWIR patch dataset is produced using the custom FAST setting scheme proposed by Aguilera et al. [2], which can produce more similar responses in the two spectra and thus generate more matching sample pairs. For the generation of non-matching sample pairs, a VIS image patch of each matching sample pair randomly selects an image patch with inconsistent keypoint coordinates from the corresponding LWIR image. The dataset contains a total of 21,370 pairs with equal numbers of positive and negative samples, of which the training set contains 17,096 pairs and the test set contains 4,274 pairs. Fig. 2 shows some samples from the VIS-LWIR patch dataset, where the size of each image patch is 64×64 pixels. By comparing Fig. 1 and Fig. 2, it can be seen that the non-linear difference of VIS-LWIR is more significant than that of VIS-NIR. At the same time, LWIR images contain less detailed information than VIS images.

3) *OS patch dataset*. It is a VIS-SAR image patch matching dataset constructed by Yu et al. based on the OS dataset [4]. The dataset contains 123,676 pairs with equal numbers of positive and negative samples. The training set contains 98,940 pairs, and the test set contains 24,736 pairs. Each 64×64 pixel image patch is cropped around the keypoint extracted by the SIFT method. Pairs of VIS and SAR image patches with the same keypoints are considered matching samples. The image patch pairs with different keypoints are regarded as non-matching samples. Fig. 3 shows some samples from the OS patch dataset. From Figs. 1-3, compared with the VIS-NIR and VIS-LWIR cross-spectral image patch matching scenarios, the VIS-SAR image patch pairs show more significant non-linear differences. In addition, there is severe speckle noise in SAR images, which makes it more difficult to extract effective features.

## B. More Experiments

In this section, we provide more experiments to explore our KGL-Net in more detail, including the ECA module [13] in the feature extraction network part, feature difference learning in the metric branch, the learning rate optimization strategy, the descriptor length, the combined network architecture and the HNSM-M strategy.

1) *ECA module*. Different from target detection and target segmentation tasks, which require precise positioning

Table 6. Comparison of different combined network architectures on the VIS-NIR patch dataset.

Scheme	Field	Forest	Indoor	Mountain	Oldbuilding	Street	Urban	Water	Mean
Combined Network Architectures - Series A									
A1 w/o HNSM-M	2.27	0.09	1.22	0.91	1.05	0.58	0.77	<b>1.79</b>	1.09 (-33.0%)
<b>A1 w/ HNSM-M</b>	<b>1.52</b>	<b>0.03</b>	<b>0.55</b>	<b>0.54</b>	<b>0.61</b>	<b>0.26</b>	<b>0.34</b>	1.97	<b>0.73</b>
A2 w/o HNSM-M	2.10	0.12	1.25	0.84	0.73	0.50	0.37	<b>1.94</b>	0.98 (-6.1%)
<b>A2 w/ HNSM-M</b>	<b>1.98</b>	<b>0.05</b>	<b>1.04</b>	<b>0.42</b>	<b>0.58</b>	<b>0.29</b>	<b>0.30</b>	2.67	<b>0.92</b>
A3 w/o HNSM-M	1.64	0.08	1.08	0.54	0.63	0.31	0.53	<b>1.91</b>	0.84 (-20.2%)
<b>A3 w/ HNSM-M</b>	<b>1.14</b>	<b>0.03</b>	<b>0.73</b>	<b>0.37</b>	<b>0.56</b>	<b>0.22</b>	<b>0.22</b>	2.13	<b>0.67</b>
A4 w/o HNSM-M	1.83	0.09	1.29	0.83	0.87	0.46	0.66	1.68	0.96 (-26.0%)
<b>A4 w/ HNSM-M</b>	<b>1.42</b>	<b>0.03</b>	<b>0.95</b>	<b>0.38</b>	<b>0.68</b>	<b>0.29</b>	<b>0.29</b>	<b>1.63</b>	<b>0.71</b>
Combined Network Architectures - Series B									
B1 w/o HNSM-M	2.39	0.13	1.41	1.04	0.74	0.59	0.58	<b>1.64</b>	1.07 (-6.5%)
<b>B1 w/ HNSM-M</b>	<b>2.09</b>	<b>0.09</b>	<b>1.36</b>	<b>0.88</b>	<b>0.67</b>	<b>0.71</b>	<b>0.38</b>	1.81	<b>1.00</b>
B2 w/o HNSM-M	<b>3.10</b>	0.20	1.87	1.45	1.05	0.68	0.54	2.66	1.44 (-20.1%)
<b>B2 w/ HNSM-M</b>	3.14	<b>0.13</b>	<b>1.42</b>	<b>0.76</b>	<b>0.65</b>	<b>0.54</b>	<b>0.38</b>	<b>2.15</b>	<b>1.15</b>
B3 w/o HNSM-M	1.77	0.09	1.86	0.81	0.73	0.45	0.41	2.01	1.02 (-19.6%)
<b>B3 w/ HNSM-M</b>	<b>1.73</b>	<b>0.09</b>	<b>1.30</b>	<b>0.58</b>	<b>0.59</b>	<b>0.32</b>	<b>0.23</b>	<b>1.71</b>	<b>0.82</b>
B4 w/o HNSM-M	3.59	0.15	1.29	1.15	0.75	0.64	0.48	<b>1.67</b>	1.22 (-16.4%)
<b>B4 w/ HNSM-M</b>	<b>2.85</b>	<b>0.10</b>	<b>1.06</b>	<b>0.69</b>	<b>0.68</b>	<b>0.51</b>	<b>0.40</b>	1.83	<b>1.02</b>
Combined Network Architectures - Series C									
C1 w/o HNSM-M	1.95	0.10	0.98	0.76	0.92	0.55	0.61	1.59	0.93 (-35.5%)
<b>C1 w/ HNSM-M</b>	<b>1.37</b>	<b>0.04</b>	<b>0.63</b>	<b>0.41</b>	<b>0.51</b>	<b>0.28</b>	<b>0.22</b>	<b>1.38</b>	<b>0.60</b>
C2 w/o HNSM-M	2.29	0.15	1.21	0.77	0.64	0.44	0.35	2.01	0.98 (-37.8%)
<b>C2 w/ HNSM-M</b>	<b>1.09</b>	<b>0.04</b>	<b>0.63</b>	<b>0.35</b>	<b>0.50</b>	<b>0.26</b>	<b>0.21</b>	<b>1.81</b>	<b>0.61</b>
C3 w/o HNSM-M	1.91	0.11	1.14	0.64	0.59	0.42	0.36	<b>1.34</b>	0.81 (-33.3%)
<b>C3 w/ HNSM-M</b>	<b>1.00</b>	<b>0.03</b>	<b>0.83</b>	<b>0.28</b>	<b>0.47</b>	<b>0.20</b>	<b>0.17</b>	1.37	<b>0.54</b>
C4 w/o HNSM-M	1.82	0.17	1.26	0.93	0.64	0.62	0.45	2.25	1.02 (-37.3%)
<b>C4 w/ HNSM-M</b>	<b>1.42</b>	<b>0.05</b>	<b>0.90</b>	<b>0.29</b>	<b>0.46</b>	<b>0.24</b>	<b>0.25</b>	<b>1.49</b>	<b>0.64</b>
C5 w/o HNSM-M	1.78	0.14	0.95	0.75	0.65	0.56	0.50	1.75	0.88 (-31.8%)
<b>C5 w/ HNSM-M</b>	<b>1.33</b>	<b>0.03</b>	<b>0.55</b>	<b>0.30</b>	<b>0.49</b>	<b>0.24</b>	<b>0.24</b>	<b>1.62</b>	<b>0.60</b>
C6 w/o HNSM-M	1.86	0.12	1.39	0.77	0.86	0.49	0.64	1.65	0.97 (-25.8%)
<b>C6 w/ HNSM-M</b>	<b>1.64</b>	<b>0.04</b>	<b>0.86</b>	<b>0.47</b>	<b>0.61</b>	<b>0.33</b>	<b>0.35</b>	<b>1.46</b>	<b>0.72</b>
Combined Network Architectures - Series D									
D1 w/o HNSM-M	3.80	0.34	1.71	1.68	0.93	0.89	0.63	1.98	1.49 (-35.6%)
<b>D1 w/ HNSM-M</b>	<b>1.97</b>	<b>0.08</b>	<b>1.22</b>	<b>0.73</b>	<b>0.83</b>	<b>0.54</b>	<b>0.56</b>	<b>1.76</b>	<b>0.96</b>
D2 w/o HNSM-M	3.45	0.42	2.67	1.74	1.13	0.87	0.73	2.98	1.75 (-38.9%)
<b>D2 w/ HNSM-M</b>	<b>2.79</b>	<b>0.10</b>	<b>1.41</b>	<b>0.58</b>	<b>0.61</b>	<b>0.60</b>	<b>0.29</b>	<b>2.17</b>	<b>1.07</b>
D3 w/o HNSM-M	3.21	0.10	2.64	1.41	0.87	0.56	0.59	2.78	1.52 (-39.5%)
<b>D3 w/ HNSM-M</b>	<b>2.26</b>	<b>0.08</b>	<b>1.27</b>	<b>0.56</b>	<b>0.47</b>	<b>0.47</b>	<b>0.37</b>	<b>1.85</b>	<b>0.92</b>
D4 w/o HNSM-M	2.67	0.18	2.33	1.08	0.90	0.89	0.59	<b>2.08</b>	1.34 (-17.9%)
<b>D4 w/ HNSM-M</b>	<b>2.67</b>	<b>0.10</b>	<b>1.72</b>	<b>0.61</b>	<b>0.70</b>	<b>0.53</b>	<b>0.35</b>	2.09	<b>1.10</b>
D5 w/o HNSM-M	2.67	0.18	1.73	0.99	0.84	0.72	0.56	<b>2.24</b>	1.24 (-21.0%)
<b>D5 w/ HNSM-M</b>	<b>2.09</b>	<b>0.06</b>	<b>1.15</b>	<b>0.54</b>	<b>0.78</b>	<b>0.45</b>	<b>0.35</b>	2.38	<b>0.98</b>
D6 w/o HNSM-M	2.94	0.15	1.70	1.32	0.91	0.65	0.64	1.91	1.28 (-30.5%)
<b>D6 w/ HNSM-M</b>	<b>1.95</b>	<b>0.11</b>	<b>1.38</b>	<b>0.71</b>	<b>0.72</b>	<b>0.39</b>	<b>0.41</b>	<b>1.41</b>	<b>0.89</b>

of target boundary pixels, image patch matching focuses on measuring the similarity between image patches. For an image patch with a size of only  $64 \times 64$  pixels, the effective local features that can be extracted are limited. Fully considering the global features of image patches will be more helpful in extracting richer effective features. At the same time, we aim to build a lightweight network. Therefore, a lightweight ECA module is selected and reasonably embedded into the network we constructed. From Table 1, on the three datasets of different cross-spectral scenarios, the use of the ECA module can

reduce FPR95 by 5.4%-7.3% compared with not using the ECA module. This shows that more attention should be paid to global context features for this task.

2) *Feature difference learning in the metric branch.* To further verify the effectiveness of using feature difference learning in the metric branch of KGL-Net, we compare it with feature product learning [5] and feature concatenation learning [5]. From Table 2, compared with feature product learning and feature concatenation learning, feature difference learning can reduce FPR95 by 20.6% and 16.9%, respectively. On the one hand, it shows that feature

difference learning is better than feature product learning that focuses on extracting consistent features and feature concatenation learning that focuses on extracting general features. On the other hand, it shows that the metric learning based on feature difference learning and the descriptor learning based on Euclidean distance have feature extraction consistency. In addition, we can find that the results of feature product learning and feature concatenation learning can also achieve better results than the previous excellent FIL-Net [3]. The reason is that although they do not have feature extraction consistency with descriptor learning based on the Euclidean distance, hard samples are often difficult overall. Therefore, the knowledge of hard samples provided by the descriptor network can still play a certain role for them, but the performance will be relatively poor. This also further verifies the effectiveness of our HNSM-M strategy.

**3) Learning rate optimization strategy.** To further explore the impact of the learning rate optimization strategy on the performance of the final generated model, we conduct experiments on KGL-Net with various learning rate optimization strategy settings. The experimental results are shown in Table 3. The number of cycles in the ‘‘Cosine annealing’’ experiment [14] is one quarter of the total number of epochs. In the ‘‘Simulated annealing’’ [15] experiment, the initial epoch is set to 2 and the annealing conditions increase sequentially by a factor of 2. Compared with not using the learning rate optimization strategy, using cosine annealing and simulated annealing can reduce FPR95 by 5.6% (from 0.54 to 0.51) and 1.9% (from 0.54 to 0.53), respectively. Notably, the results of KGL-Net in the main paper do not use any learning rate optimization strategy. In the main paper, we focus more on exploring a stable and efficient bridge between descriptor learning and metric learning and the actual performance improvement it brings. The results in Table 3 verify that a reasonable learning rate optimization strategy can further improve performance.

**4) Descriptor length.** To further explore the impact of the descriptor length of the descriptor network output on the performance of the final generative model, we conduct experiments on KGL-Net with various descriptor length settings. The experimental results are shown in Table 4. It can be found that when the descriptor length is longer, the performance of the final model is enhanced. The longer the descriptor length is, the more global information it can express, which enables more sophisticated selection of hard negative samples and thus enhances model performance. Notably, consistent with previous studies [16-18], the results of KGL-Net in the main paper are based on a descriptor length of 128. The results in Table 4 verify that a reasonable increase in the descriptor length helps further improve the performance.

**5) Combined network architecture and the HNSM-M strategy.** To further explore the performance of the

combined network architecture between descriptor learning and metric learning and our proposed HNSM-M strategy, we present in detail the results of 20 combined network architectures before and after the use of the HNSM-M strategy on the VIS-NIR patch dataset and VIS-LWIR patch dataset. From Table 5 and Table 6, the series C has significantly better performance. This shows that when the metric network and the descriptor network share parameters in the front network layer but do not share parameters in the back network layer, better combined network performance can be achieved. Among them, when the descriptor network is a Siamese structure and the metric network is a Pseudo-Siamese structure, the architecture (C3) has a unified optimal performance. This can provide some guidance for subsequent bridge design. In addition, compared with not using our proposed HNSM-M strategy, using this strategy can reduce the FPR95 by 3.8%-55.9% on the VIS-LWIR patch dataset and can reduce the FPR95 by 6.5%-39.5% on the VIS-NIR patch dataset. Furthermore, by observing the comparison results of each subset in Table 6, the use of the HNSM-M strategy can achieve performance improvements on almost all the subsets, especially for the difficult ‘‘Field’’ subset.

## C. More Discussion

For the performance bottleneck of current cross-spectral image patch matching research, we break away from the inertial thinking of building a more complex feature relation extraction network structure and make the first attempt to explore a stable and efficient bridge between descriptor learning and metric learning. To ensure the stability and efficiency of the combined network, our KGL-Net fully considers the advantages of descriptor learning and metric learning and comprehensively builds an effective bridge from the three parts of the front, middle and back. Specifically, **firstly**, the front network layers of the descriptor network and the metric network are shared to extract sufficient low-level detail features in the front part. **Secondly**, the proposed feature-guided loss can promote the mutual guidance of features in the middle part. **Finally**, our proposed HNSM-M strategy takes advantage of the descriptor to select the hard negative sample location index to guide metric learning to achieve hard negative sample mining in the latter part. Notably, our KGL-Net achieves amazing performance improvements while abandoning complex network structures. At the same time, it is the first time that hard negative sample mining for metric networks is implemented and brings significant performance gains.

Although our KGL-Net achieves excellent performance, it is only the starting point, not the end. There are still some shortcomings in this paper. For example, the positive benefits of focusing on global features for this task have not been fully explored, the feature-guided loss only uses a simple  $L_2$  norm, and the relationship between descriptor

learning and metric learning needs to be further explored. Therefore, in the future, we will focus on global features, more effective knowledge-guided methods, and further explore the deeper relationship between descriptor learning and metric learning.

## References

- [1] Matthew Brown and Sabine Süsstrunk. Multi-spectral SIFT for scene category recognition. In *Proceedings of the IEEE Conference on Computer Vision and Pattern Recognition (CVPR)*, pages 177-184, 2011. 1, 2
- [2] Cristhian A. Aguilera, Francisco J. Aguilera, Angel D. Sappa, Cristhian Aguilera, and Ricardo Toledo. Learning Cross-Spectral Similarity Measures with Deep Convolutional Neural Networks. In *Proceedings of the IEEE Conference on Computer Vision and Pattern Recognition Workshops (CVPRW)*, pages 267-275, 2016. 1, 2
- [3] Chuang Yu, Yunpeng Liu, Jinmiao Zhao, Shuhang Wu, and Zhuhua Hu. Feature Interaction Learning Network for Cross-Spectral Image Patch Matching. *IEEE Transactions on Image Processing*, 32: 5564-5579, 2023. 1, 2, 4
- [4] Yuming Xiang, Rongshu Tao, Feng Wang, Hongjian You, and Bing Han. Automatic registration of optical and SAR images via improved phase congruency model. *IEEE Journal of Selected Topics in Applied Earth Observations and Remote Sensing*, 13: 5847-5861, 2020. 1, 2
- [5] Chuang Yu, Jinmiao Zhao, Yunpeng Liu, Shuhang Wu, and Chenxi Li. Efficient Feature Relation Learning Network for Cross-Spectral Image Patch Matching. *IEEE Transactions on Geoscience and Remote Sensing*, 61: 1-17, 2023. 1, 2, 3
- [6] David G. Lowe. Distinctive image features from scale-invariant keypoints. *International Journal of Computer Vision*. 60(2): 91-110, 2004. 2
- [7] Dou Quan, Shuang Wang, Yi Li, Bowu Yang, Ning Huyan, Jocelyn Chanussot, Biao Hou, and Licheng Jiao. Multi-Relation Attention Network for Image Patch Matching. *IEEE Transactions on Image Processing*, 30: 7127-7142, 2021. 2
- [8] Dou Quan, Shuai Fang, Xuefeng Liang, Shuang Wang, and Licheng Jiao. Cross-spectral image patch matching by learning features of the spatially connected patches in a shared space. In *Proceedings of the Asian Conference on Computer Vision (ACCV)*, pages 115-130, 2018. 2
- [9] Dou Quan, Xuefeng Liang, Shuang Wang, Shaowei Wei, Yanfeng Li, Ning Huyan, and Licheng Jiao. AFD-Net: Aggregated feature difference learning for cross-spectral image patch matching. In *Proceedings of the IEEE International Conference on Computer Vision (ICCV)*, pages 3017-3026, 2019. 2
- [10] Dou Quan, Shuang Wang, Ning Huyan, Jocelyn Chanussot, Ruoqing Wang, Xuefeng Liang, Biao Hou, and Licheng Jiao. Element-Wise Feature Relation Learning Network for Cross-Spectral Image Patch Matching. *IEEE Transactions on Neural Networks and Learning Systems*, 33(8): 3372-3386, 2021. 2
- [11] Chuang Yu, Yunpeng Liu, Chenxi Li, Lin Qi, Xin Xia, Tianci Liu, and Zhuhua Hu. Multibranch Feature Difference Learning Network for Cross-Spectral Image Patch Matching. *IEEE Transactions on Geoscience and Remote Sensing*, 60: 1-15, 2022. 2
- [12] Yeongmin Ko, Yong-jun Jang, Vinh Quang Dinh, Hae-Gon Jeon, and Moongu Jeon. Spectral-invariant matching network. *Information Fusion*, 91: 623-632, 2023. 2
- [13] Qilong Wang, Banggu Wu, Pengfei Zhu, Peihua Li, Wangmeng Zuo, and Qinghua Hu. ECA-Net: Efficient Channel Attention for Deep Convolutional Neural Networks. In *Proceedings of the IEEE Conference on Computer Vision and Pattern Recognition (CVPR)*, pages 11531-11539, 2020. 2
- [14] Ilya Loshchilov, Frank Hutter. SGDR: Stochastic Gradient Descent with Warm Restarts. In *Proceedings of the International Conference on Learning Representations (ICLR)*, 2017. 4
- [15] Scott Kirkpatrick, Daniel C Gelatt, and Mario P Vecchi. Optimization by Simulated Annealing. *Science*, 220(4598): 671-680, 1983. 4
- [16] Yurun Tian, Bin Fan, and Fuchao Wu. L2-Net: Deep learning of discriminative patch descriptor in Euclidean space. In *Proceedings of the IEEE Conference on Computer Vision and Pattern Recognition (CVPR)*, pages 661 -669, 2017. 4
- [17] Yurun Tian, Xin Yu, Bin Fan, Fuchao Wu, Huub Heijnen, and Vassileios Balntas. SOSNet: Second order similarity regularization for local descriptor learning. In *Proceedings of the IEEE Conference on Computer Vision and Pattern Recognition (CVPR)*, pages 11008–11017, 2019. 4
- [18] Yurun Tian, Axel Barroso-Laguna, Tony Ng, Vassileios Balntas, and Krystian Mikolajczyk. HyNet: Learning local descriptor with hybrid similarity measure and triplet loss. In *Proceedings of the Advances in Neural Information Processing Systems (NeurIPS)*, pages 1-12, 2020. 4